# Pulse shaping using dispersion-engineered difference frequency generation

M. Allgaier ●,[1] V. Ansari,[1] J. M. Donohue,[1,2] C. Eigner,[1] V. Quiring,[1] R. Ricken,[1] B. Brecht,[1] and C. Silberhorn[1]

[1]*Integrated Quantum Optics, Applied Physics, University of Paderborn, 33098 Paderborn, Germany*

[2]*Institute for Quantum Computing, University of Waterloo, 200 University Avenue West, Waterloo, Ontario, Canada N2L 3G1*

The temporal-mode (TM) basis is a prime candidate to perform high-dimensional quantum encoding. Quantum frequency conversion has been employed as a tool to perform tomographic analysis and manipulation of ultrafast states of quantum light necessary to implement a TM-based encoding protocol. While demultiplexing of such states of light has been demonstrated in the quantum pulse gate (QPG), a multiplexing device is needed to complete an experimental framework for TM encoding. In this work we demonstrate the reverse process of the QPG. A dispersion-engineered difference frequency generation in nonlinear optical waveguides is employed to imprint the pulse shape of the pump pulse onto the output. We study experimentally the process by spectrally shaping the first five orders of Hermite-Gauss modes of various bandwidths. Finally, we establish and model the limits of practical, reliable spectral pulse shaping operation.

## I. INTRODUCTION

High-dimensional encoding can potentially increase the security of quantum communication protocols as well as the information capacity of a single photon [1,2]. Orbital angular momentum (OAM) has been proposed as such a basis for high-dimensional encoding [3] but is inherently incompatible with existing telecommunication fiber networks. Temporal modes (TMs) of ultrafast pulses of light are a viable fiber-compatible alternative to OAM, owing to their spatially single-mode nature [4]. The core of the TM framework is the quantum pulse gate (QPG), a nonlinear optical device based on dispersion-engineered quantum frequency conversion in nonlinear waveguides [5]. The QPG has been shown to perform efficient sorting, i.e., demultiplexing, of the orthogonal but field-overlapping modes [6–12], as well as state manipulation and purification [9], photon subtraction [13,14], and noise suppression [15]. Quantum light in a TM basis can be directly generated using an adapted parametric down-conversion source [16]. For two-dimensional states, reshaping, i.e., modal rotation, has been explored [17]. However, an independent TM multiplexing device capable of arbitrary TM shaping and reshaping of higher-order modes such as the quantum pulse shaper (QPS) described in Ref. [18] has not been demonstrated either on the single-photon level or classically. Such a device, together with a QPG, could perform rotations between TMs. Both devices together would form a framework for TM-based quantum communication [4,19]. Shaping of arbitrary spectra is possible. The process can in principle be very efficient, contrary to established classical pulse shaping methods in the spectral [20] and time domain [21], which carve the desired pulse shape from a more broad-band input spectrum or temporal envelope.

In this work we experimentally demonstrate a pulse shaper based on difference frequency generation (DFG) and study its performance using coherent light. We verify successful shaping of continuous-wave light into the first five orders of Hermite-Gauss modes using spectral intensity measurements.

We assess the process's shaping accuracy by scanning the bandwidth of the desired spectrum and model experimental imperfections for comparison. We thus establish a range of working parameters for such a pulse reshaping device. We demonstrate that the device can be implemented in the same dispersion-engineered waveguides as the QPG. Establishing these limits is an important step towards implementing a QPS using such a tailored DFG process.

## II. DESIGN OF THE NONLINEAR PROCESS

To design a DFG pulse shaping device such as the QPS, one has to first revisit the working principle behind the QPG. Key to the QPG device is its unique group-velocity relationship: By matching the group velocity of the input and pump field in a sum-frequency generation (SFG) process, the conversion efficiency is directly proportional to the temporal overlap of the two fields, thus allowing selective conversion of field-orthogonal modes. This group-velocity matching has been achieved in two different ways: using an almost degenerate type-0 nonlinear process [10,11] or by compensating for the waveguide's dispersion with material birefringence using a type-II process [18]. The latter has the prospect of better background suppression, resulting in a signal-to-noise ratio sufficient for operating on quantum light [9]. This particular type-II implementation addresses inputs in the telecom band around 1550 nm and outputs them in the visible range around 557 nm. A QPS should ideally work in the opposite direction, thus enabling us to reconvert the output of a QPG to allow for TM rotations. Therefore, we propose to employ the reverse process of the QPG, i.e., DFG. Here, the use of a type-II process is especially advantageous over a type-0 one: The single-photon output at 1550 nm for a type-0 process can be separated from its pump field only by a few nanometers and therefore be polluted by Raman-scattered photons. The process is implemented in periodically poled lithium niobate waveguides. Employing the exact reverse process for SFG and DFG, i.e., the same material, wavelengths, and polarizations,
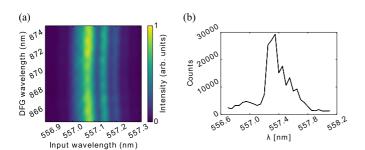
(a)

(b)



FIG. 1. (a) DFG phase matching derived from the measured SFG phase matching. (b) Phase-matching scan at a cw pump wavelength of 1550 nm.

allows the usage of the same waveguide structure and poling period. For group-velocity matched SFG, highly efficient bandwidth compression has already been demonstrated [22]. In an analogous fashion, pulse shaping implemented in the DFG process can also be highly efficient and even bandwidth expansion is possible, with potential applications in interfacing with narrowband photons.

## III. EXPERIMENTAL SETUP

For the DFG device presented here, a central pump wavelength of 1550 nm is chosen in order to convert narrowband light at 557 nm to 850 nm. This interchange of pump and output wavelength is possible due to the matched group velocity, and the necessary lasers and classical pulse shapers were already available to the authors. From the SFG phase matching measured using the reverse process (SFG configuration) [22], we derive the corresponding DFG phase matching shown in Fig. 1. The SFG phase matching was measured using a tunable cw laser at 1550 nm together with a broadband pulsed pump at 850 nm. The spectrum of the converted light was then recorded for every setting of the tunable laser. The spectra were finally stitched together. Since DFG is the reverse process of SFG, the corresponding phase matching can be derived from the SFG measurement by rotating and rescaling the image. To verify that the resulting image is correct, we perform a scan at a fixed pump wavelength of 1550 nm, shown in Fig. 1(b).

Transferring pulse shapes through DFG has been demonstrated before for midinfrared pulse shaping [23]. Such implementations must contend with the fact that the desired spectrum gets convoluted with the Gaussian pump spectrum. The distinct asymmetric phase-matching condition used in this work (as shown in Fig. 1) circumvents the problem by filtering of the input spectra, thus strongly limiting the convolution of the two input spectra.

The experimental setup is shown in Fig. 2. To generate the input light we rely on a diode-pumped solid-state laser emitting at 514 nm to pump a standing-wave continuous-wave dye laser. Rhodamine 560 is employed as a laser dye to generate the necessary wavelength of 557 nm at an average power output of 60 mW. The laser's emission bandwidth is typically of the order of 5 GHz. A pulsed laser at 550 nm was not available to the authors. The pump pulses are generated with a cascade of a Ti:sapphire oscillator operating at an 80-MHz repetition rate and an optical parametric oscillator
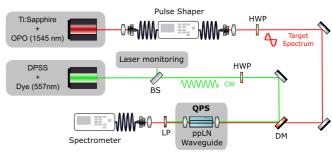


FIG. 2. Experimental setup for device characterization. The following denotations are used: OPO, optical parametric oscillator; DPSS, diode-pumped solid-state laser; HWP, half waveplate; Ti:ppLN, periodically poled lithium niobate; and LP, long pass filter. All fibers are SMF-28 single-mode fibers.

emitting pulses with a central wavelength of 1550 nm. The light is coupled to standard SMF-28 fibers and fed through a fiber-coupled spatial light modulator-based pulse shaper (Finisar Waveshaper 4000s) with a resolution of 10 GHz over the entire telecom *C* band. The pulses with a pulse energy of the order of 25 pJ (depending on the pulse shape) are combined with the 557-nm input light on a dichroic mirror and coupled into a 27-mm-long, homemade titanium-indiffused lithium niobate waveguide with a poling period of 4.4 $\mu$m, temperature stabilized at 190 °C. Input and pump pulses are orthogonally polarized since we are employing a type-II process. The converted light is separated from the input light and coupled to another single-mode fiber. We employ a single-photon sensitive spectrometer with a resolution of 0.05 nm at 870 nm, provided by a 1200-line/mm grating. For analysis, we calculate the expected DFG spectrum from the spectrum programmed on the pulse shaper. This is particularly simple due to the continuous-wave input. We compare this spectrum to the measured one by means of an overlap integral. The purpose of this measurement is to establish the range of parameters for which the DFG process can imprint the programmed pulse shape onto the converted light. Unfortunately, with the available input and pump power, the generated pulses are too weak to characterize their spectral phase using classical pulse characterization techniques.

Light produced by parametric down-conversion sources naturally decomposes into the Hermite-Gauss basis [24]. Since the device presented here is intended for use in the QPG framework, we choose exactly this basis. The spectral envelope of the pulses reads

$$\text{HG}_n(\lambda) = \frac{H_n(\lambda - \lambda_0)}{N_n} e^{-(\lambda - \lambda_0)^2 / 2\sigma^2}, \tag{1}$$

where $H_n$ denotes the Hermite polynomial of order $n$, $\lambda_0$ is the central wavelength, and $\sigma$ denotes the base Gaussian bandwidth in the following, although the actual spectral spread will be higher for higher-order modes. In addition, $N_n$ normalizes the Hermite-Gauss function. We scan the bandwidth $\sigma$ of the underlying Gaussian [compare with Eq. (1)] from 0.25 nm to 10 nm in steps of 0.25 nm and perform eight measurements with a 4-s integration time each for every set of parameters. The standard deviation over the mean value of the eight measurements is used to generate error bars. Thus, for every Hermite-Gauss order 320 measurements are taken; this task
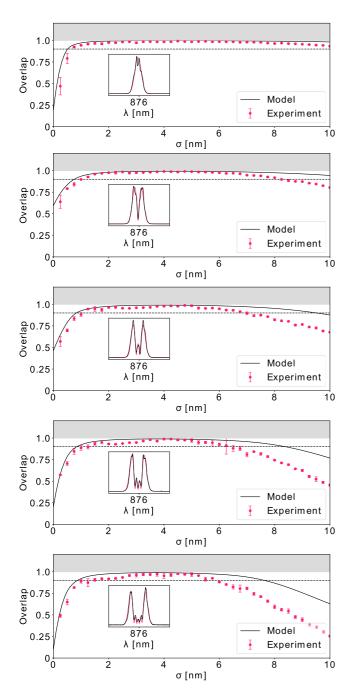
FIG. 3. Overlap between the programmed and measured Hermite-Gauss spectra for the first five modes as a function of the Gaussian bandwidth $\sigma$ [compare with Eq. (1)]. The dashed lines indicate 95 % overlap. Solid lines indicate the overlap between the programmed and modeled spectra, which include experimental limitations. The insets show the programmed (magenta) and measured (black) spectra for each mode and a bandwidth of 5 nm.

is repeated for the first five orders of Hermite-Gauss modes over the course of half a day. For every bandwidth $\sigma$, we calculate the overlap integral $\mathcal{O}$ between the area-normalized programmed and measured spectra

$$\mathcal{O} = \frac{\left(\int S(\lambda)T(\lambda)d\lambda\right)^2}{\int S^2(\lambda)d\lambda \int T^2(\lambda)d\lambda}, \qquad (2)$$
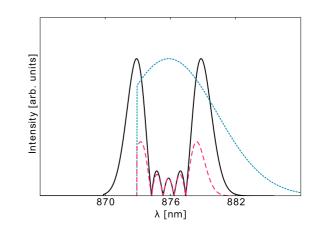


FIG. 4. Sketched programmed spectrum (black, solid line), available Gaussian OPO spectrum with limited shaper range (blue dotted line), and theoretically resulting actual pump spectrum (magenta dashed line) for a fourth-order Hermite-Gauss mode. Cutting occurs at the upper edge of the $C$ band (1565 nm), which appears inverted at the lower end of the spectrum after DFG.

where $S(\lambda)$ and $T(\lambda)$ are the measured and programmed spectra, respectively, taken about their respective central wavelengths. The programmed spectrum at the DFG output is calculated by taking the spectrum programmed on the pulse shaper and merely shifting it, since a monochromatic input for the DFG is assumed. The results are displayed in Fig. 3.

## IV. RESULTS

The overlap between the measured programmed spectra is displayed in magenta. The achieved overlap is above 90% over a large bandwidth range from about 1 to 6 nm for all five modes. The best overlap at over 95% is achieved for bandwidths between roughly 3.5 and 5 nm. This is convenient, since other components like the QPG and parametric down-conversion sources also work well within this range, since they can be based on similar waveguides [10–12]. It is noteworthy that a higher-order Hermite-Gauss mode of the same nominal bandwidth occupies a wider spectrum, since the Gaussian is scaled by the Hermite polynomial. This causes the steeper decline of the overlap for wider bandwidths and higher orders. To better understand these results, we modeled the experimental limitations of the current setup. The overlap between these modeled spectra and the programmed ones is again calculated and displayed as solid lines. The model contains two classes of contributions.

First, we account for insufficiently available bandwidth from the optical parametric oscillator (OPO) at 1550 nm, which effectively narrows down the shaped spectrum. This includes three contributions: the available bandwidth from the pump laser, the available phase-matching bandwidth, and the range of the pulse shaper. While the first two contributions result in a combined Gaussian spectrum of 10-nm FWHM, with which the programmed spectrum is multiplied, the third contribution of the pulse shaper cuts off part of the spectrum for large bandwidths $\sigma$. This is discussed further in the Appendixes. Figure 4 shows this effect for the fourth-order mode with a bandwidth of 10 nm. The black line is the programmed spectrum. However, it can only be carved within

the limited operating bandwidth of the pulse shaper, which cuts the Gaussian spectrum of the OPO light at the upper edge of the *C* band (1565 nm), reflecting to the lower end of the DFG spectrum (shown in blue, cut outside the shaping range), which is why the actual shaped spectrum (magenta) looks different from the programmed one. The difference is mostly visible in the outer parts of the spectrum, which is why only large bandwidths and higher-order modes are affected.

Second, we model convolution effects. These are due to limited resolution of the employed pulse shaper (10 GHz) and spectrometer (20 GHz), as well as the non-negligible bandwidth of the dye laser (5 GHz). The programmed spectrum is convoluted with a Gaussian to account for these effects. Another such effect stems from multimodeness of the dye laser, which experiences a certain degree of mode competition. The two modes of 5-GHz bandwidth are estimated to be about 0.1 nm apart. We account for this by adding up two spectra of the same separation. We estimate the ratio to be 1:1, since the mode competition takes place on the order of seconds, whereas the measurement for each bandwidth takes 32 s, thus averaging sufficiently over both mode contributions. These effects blur the spectrum and lead to diminished overlap for small bandwidths.

It is apparent that the model does not fit well the large bandwidths, while the qualitative trend is still reproduced. We attribute this to instabilities in the spectra produced by the optical parametric oscillator. It is possible to observe fringing effects in the pump spectrum in front of the pulse shaper, manifesting as small features in the spectra. In addition, the pump spectrum in front of the pulse shaper is not exactly Gaussian and exhibits some degree of asymmetry. These features change over time on a scale of 10 s and cause more pronounced deviations for more complex and wider spectra.

The individual contributions to the model are treated in more detail in the Appendixes. From the achieved overlaps we conclude that the device works in principle, with some constraints imposed by the current experimental setup. However, it is important to dissect which of the imperfections are fundamental to the device and which are only caused by auxiliary equipment such as the lasers. First, the spectrometer resolution is not a fundamental restriction for the device, since it only influences how well the shaped spectra can be characterized, not how well they are shaped. The effects imposed by the pulse shaper are device dependent. This leaves the 557-nm input bandwidth and phase-matching bandwidth as ultimate limits to device performance. Therefore, we model the influences of these ultimate limitations on the proposed pulsed input device. The input bandwidth should always be chosen smaller than or equal to the phase-matching bandwidth or otherwise the spectrum will be cut and effectively filtered once more. We now assume a flat spectral intensity and phase of the pump laser spectrum, as well as a flat response of the pulse shaper. The pulse shaper's resolution of 10 GHz will be small compared to the phase-matching bandwidth and neglected. Still, the nonzero input bandwidth results in a convolution effect just like the ones discussed above. Using those benchmark numbers, calculations identical to the model already presented were prepared to simulate the effect of the input and phase-matching bandwidth on the quantum device performance. This simulation assumes a broadband input as
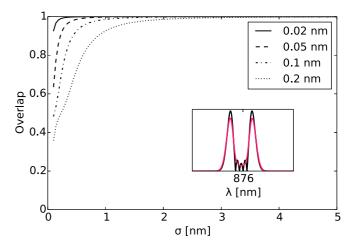


FIG. 5. Overlap between the programmed and modeled spectra of the fourth Hermite-Gauss order for various phase-matching bandwidths. The inset shows the programmed (black) and model (magenta) spectrum for a phase-matching bandwidth of 0.2 nm and a mode bandwidth of 1.8 nm.

one would use for quantum communication with temporal modes, where the bandwidth is equal to the phase-matching bandwidth. Since the highest-order mode used is subject to the strongest limitations, we only show the results for the fourth-order Hermite-Gauss mode in Fig. 5. It can be seen that for a more narrow phase-matching bandwidth than the one for the waveguide used in this work, shaping bandwidths under 1 nm is certainly possible. This would require longer waveguides, since the phase-matching bandwidth is in general inversely proportional to the crystal length. This is highly desirable in the light of optical fiber dispersion and spectral information density. At the same time, high shaping fidelity for small bandwidth features would also allow us to shape higher-order modes efficiently. The inset shows the programmed and model spectra for a mode bandwidth of 1.8 nm and a phase-matching bandwidth of 0.2 nm, which is roughly the phase-matching bandwidth of the employed waveguide. The blurring effect on the central features can clearly be observed. This is the source of the diminished overlap.

## V. CONCLUSION

In conclusion, we have shown the classical characterization of a DFG pulse shaper and successful reshaping of the input light into Hermite-Gauss pulses of a broad substantial range of bandwidths. From the theoretical model of the experimental imperfections we draw the conclusion that a highly functional device for pulsed operation can be implemented using the current waveguide technology.

An important aspect for future work is efficiency. The transformation is in theory unitary and can be more efficient than classical pulse shaping methods, which is especially desirable for converting single photons. The particular phase-matching condition described here, along with the adapted input pulse and phase-matching bandwidth, can also be useful as a classical arbitrary pulse shaping technique for the near-infrared and midinfrared ranges [23,25]: Since convolution with a second unshaped pulse is highly limited, high shaping resolution and pulse complexity can be achieved in principle.
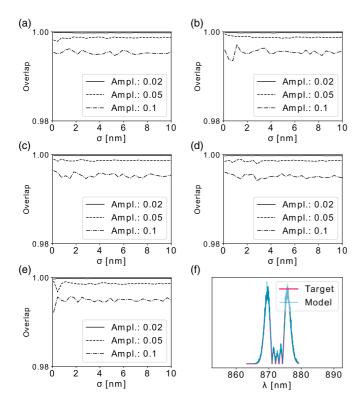
FIG. 6. (a)–(e) Overlap for modes 0–4 with different noise amplitudes. (f) Example spectrum for mode 4 with a noise amplitude of 0.1 and bandwidth of 10 nm.

### APPENDIX A: NOISE CONTRIBUTION

In the main text the role of noise on the overlap measurement was discussed. Noise was excluded from the model since its influence was negligible for reasonable amounts of noise. Figure 6 shows the overlap where the model only includes noise. An amplitude of 0.03 corresponds roughly to the amount of noise present in the measurement. The influence of noise is very uniform first over all bandwidths and second over all modes. In addition, even massive noise levels of 0.1,
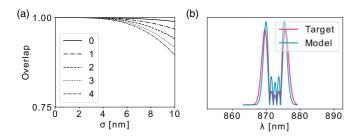


FIG. 7. (a) Overlap for the first five Hermite-Gauss modes with limited pump bandwidth, phase-matching bandwidth, and shaper range. (b) Target and model spectra for the fourth-order mode and a bandwidth of 10 nm.
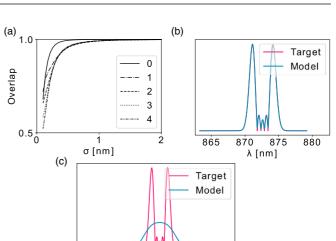


FIG. 8. (a) Overlap for the first five Hermite-Gauss modes with limited system resolution. Also shown are the target and model spectra for the fourth-order mode and a bandwidth of (b) 5 nm and (c) 0.1 nm.

as shown in Fig. 6(f), only reduce the overlap to 0.995. It is clear that the overlap as a measure of shaping fidelity is very insensitive to noise, and therefore we excluded it from the model.

### APPENDIX B: INSUFFICIENT PUMP BANDWIDTH

Figure 7 shows the influence of limited pump bandwidth on the overlap for the first five Hermite-Gauss orders. There are three components factoring into this effect. The first is a limited pump bandwidth of 17 nm and the second is a limited phase-matching bandwidth. The latter plays a minor effect with a FWHM Gaussian bandwidth of about 60 nm. Multiplied, the two result in a Gaussian bandwidth of roughly
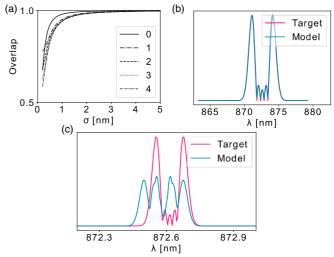


FIG. 9. (a) Overlap for the first five Hermite-Gauss modes with simulated mode competition of the laser. Also shown are the target and model spectra for the fourth-order mode and a bandwidth of (b) 5 nm and (c) 0.2 nm.

TABLE I. Contributions to the model.

| Limitation | Source | Effect on model spectrum | Bandwidth affected |
|---|---|---|---|
| limited bandwidth | pulse shaper, pump laser, phase matching | too narrow spectrum | large |
| mode competition | input laser | blurred spectrum | small to medium |
| limited resolution | spectrometer, laser, pulse shaper, phase matching | spectrum is convoluted | small |
| noise | spectrometer, pulse shaper, pump laser | overlap reduced globally | all |

10 nm. The third effect is the limited range of the pulse shaper, which has a flat response over the whole telecom $C$ band from 1530 to 1565 nm. The model spectrum $M(\lambda)$ has been calculated from the target spectrum $T(\lambda)$ as

$$M(\lambda) = F(\lambda)T(\lambda), \qquad (B1)$$

where $F$ is a filter function that describes the shape of the cutoff available spectrum.

## APPENDIX C: CONVOLUTION EFFECTS

The model spectrum $M(\lambda)$ has been calculated from the target spectrum $T(\lambda)$ as

$$M(\lambda) = \int d\lambda' T(\lambda') \exp\left(-\frac{(\lambda - \lambda_0 - \lambda')^2}{2\sigma_m^2}\right), \qquad (C1)$$

with

$$\sigma_m = \sqrt{\sigma_1^2 + \sigma_2^2 + \sigma_3^2}, \qquad (C2)$$

where $\sigma_m$ is the standard deviation describing all combined measurement uncertainties, which are the shaper and spectrometer resolution of $\sigma_1 = 5$ GHz and $\sigma_2 = 0.05$ nm, respectively, as well as the dye laser bandwidth of $\sigma_3 = 5$ GHz. The effect of this contribution to the model is shown in Fig. 8. The effect is only apparent for the smallest of bandwidths. Two examples of model spectra for the fourth order are displayed in Figs. 8(b) and 8(c). While the limited overall system resolution completely blurs the target spectrum for 0.1-nm bandwidths, the effect is barely visible for 5 nm, where it only slightly diminishes the visibility of the dips.

## APPENDIX D: MULTIMODENESS OF THE INPUT LASER

As a dummy probe, instead of a pulsed input, we are using a 514-nm pumped standing-wave dye laser, which relies on rhodamine 560 as a gain medium. Such lasers are the only emitters in the wavelength range around 550 nm and the only cw light source available to the authors at the time. A cascade of a Ti:sapphire oscillator, OPO, and homemade SHG crystal would in principle provide this wavelength, but with the oscillators available to the authors, only as a pulsed source. A cw source is, even taking the imperfections of this particular laser into account, preferable, since it allows one to probe the properties of the nonlinear process mode independently of the structure and bandwidth of the particular phase matching of the crystal used here. Therefore, it is easier to ascertain whether the desired quantum device can be implemented in principle, using the suggested process and pulse shaping.

The laser is tuned using a birefringent filter in the cavity. Within its filter passband, two cavity modes can in principle participate in lasing. The laser will jump between these competing modes on a scale of 1 s or faster. The measured spectra therefore contain contributions from both spectral lines, spaced at about 0.05 nm. The observed spectra are effectively averaged over both and the two lines contribute equally, since the exposure time of the spectrometer is larger than the timescale of the mode competition. We model this process by adding a shifted copy to the target spectrum. For small target bandwidths and features, this reduces the overlap with the target spectrum significantly. The effect for the five targeted modes is shown in Fig. 9.

The effect is very similar to the convolution effects discussed earlier. The spectrum is significantly widened and overlap is lost. This also affects mostly smaller bandwidths, but not as small as the convolution effect. For very small bandwidths, the effect is even more pronounced, however, for the shown bandwidth of 5 nm the model spectrum cannot be differentiated from the one with convolution effects. Table I gives an overview of the qualitative effect of the contributions on the model spectrum.

[1] P. P. Rohde, J. F. Fitzsimons, and A. Gilchrist, Information capacity of a single photon, Phys. Rev. A **88**, 022310 (2013).

[2] A. Hayat, X. Xing, A. Feizpour, and A. M. Steinberg, Multidimensional quantum information based on single-photon temporal wavepackets, Opt. Express **20**, 29174 (2012).

[3] J. Leach, B. Jack, J. Romero, A. K. Jha, A. M. Yao, S. Franke-Arnold, D. G. Ireland, R. W. Boyd, S. M. Barnett, and M. J. Padgett, Quantum correlations in optical angle-orbital angular momentum variables, Science **329**, 662 (2010).

[4] B. Brecht, Dileep V. Reddy, C. Silberhorn, and M. G. Raymer, Photon Temporal Modes: A Complete Framework for Quantum Information Science, Phys. Rev. X **5**, 041017 (2015).

[5] A. Eckstein, B. Brecht, and C. Silberhorn, A quantum pulse gate based on spectrally engineered sum frequency generation, Opt. Express **19**, 13770 (2011).

[6] D. V. Reddy, M. G. Raymer, C. J. McKinstrie, L. Mejling, and K. Rottwitt, Temporal mode selectivity by frequency conversion in second-order nonlinear optical waveguides, Opt. Express **21**, 13840 (2013).

[7] B. Brecht, A. Eckstein, R. Ricken, V. Quiring, H. Suche, L. Sansoni, and C. Silberhorn, Demonstration of coherent time-frequency Schmidt mode selection using dispersion-engineered frequency conversion, Phys. Rev. A **90**, 030302 (2014).

[8] V. Ansari, G. Harder, M. Allgaier, B. Brecht, and C. Silberhorn, Temporal-mode measurement tomography of a quantum pulse gate, Phys. Rev. A **96**, 063817 (2017).

[9] V. Ansari, J. M. Donohue, M. Allgaier, L. Sansoni, B. Brecht, J. Roslund, N. Treps, G. Harder, and C. Silberhorn, Tomography and Purification of the Temporal-Mode Structure of Quantum Light, Phys. Rev. Lett. **120**, 213601 (2018).

[10] P. Manurkar, N. Jain, M. Silver, Y.-P. Huang, C. Langrock, M. M. Fejer, P. Kumar, and G. S. Kanter, Multidimensional mode-separable frequency conversion for high-speed quantum communication, Optica **3**, 1300 (2016).

[11] D. V. Reddy and M. G. Raymer, Engineering temporal-mode-selective frequency conversion in nonlinear optical waveguides: from theory to experiment, Opt. Express **25**, 12952 (2017).

[12] D. Reddy and M. Raymer, High-selectivity quantum pulse gating of photonic temporal modes using all-optical Ramsey interferometry, Optica **5**, 423 (2018).

[13] V. A. Averchenko, V. Thiel, and N. Treps, Nonlinear photon subtraction from a multimode quantum field, Phys. Rev. A **89**, 063808 (2014).

[14] Y.-S. Ra, C. Jacquard, A. Dufour, C. Fabre, and N. Treps, Tomography of a Mode-Tunable Coherent Single-Photon Subtractor, Phys. Rev. X **7**, 031012 (2017).

[15] A. Shahverdi, Y. M. Sua, L. Tumeh, and Y.-P. Huang, Quantum parametric mode sorting: Beating the time-frequency filtering, Sci. Rep. **7**, 6495 (2017).

[16] V. Ansari, E. Roccia, M. Santandrea, M. Doostdar, C. Eigner, L. Padberg, I. Gianani, M. Sbroscia, J. M. Donohue, L. Mancino, M. Barbieri, and C. Silberhorn, Heralded generation of high-purity ultrashort single photons in programmable temporal shapes, Opt. Express **26**, 2764 (2018).

[17] P. Manurkar, N. Jain, P. Kumar, and G. S. Kanter, Programmable optical waveform reshaping on a picosecond timescale, Opt. Lett. **42**, 951 (2017).

[18] B. Brecht, A. Eckstein, A. Christ, H. Suche, and C. Silberhorn, From quantum pulse gate to quantum pulse shaper-engineered frequency conversion in nonlinear optical waveguides, New J. Phys. **13**, 065029 (2011).

[19] V. Ansari, J. M. Donohue, B. Brecht, and C. Silberhorn, Tailoring nonlinear processes for quantum optics with pulsed temporal-mode encodings, Optica **5**, 534 (2018).

[20] A. M. Weiner, Ultrafast optical pulse shaping: A tutorial review, Opt. Commun. **284**, 3669 (2011).

[21] C. E. Rogers and P. L. Gould, Nanosecond pulse shaping at 780 nm with fiber-based electro-optical modulators and a double-pass tapered amplifier, Opt. Express **24**, 2596 (2016).

[22] M. Allgaier, V. Ansari, L. Sansoni, C. Eigner, V. Quiring, R. Ricken, G. Harder, B. Brecht, and C. Silberhorn, Highly efficient frequency conversion with bandwidth compression of quantum light, Nat. Commun. **8**, 14288 (2017).

[23] T. Witte, K. L. Kompa, and M. Motzkus, Femtosecond pulse shaping in the mid infrared by difference-frequency mixing, Appl. Phys. B **76**, 467 (2003).

[24] S. P. Walborn and A. H. Pimentel, Generalized Hermite-Gauss decomposition of the two-photon state produced by spontaneous parametric down conversion, J. Phys. B **45**, 165502 (2012).

[25] H.-S. Tan, E. Schreiber, and W. S. Warren, High-resolution indirect pulse shaping by parametric transfer, Opt. Lett. **27**, 439 (2002).